Physics Letters B 714 (2012) 215–223

Contents lists available at SciVerse ScienceDirect

Physics Letters B

www.elsevier.com/locate/physletb

Measurement of the cross-section ratio $\sigma(\chi_{c2})/\sigma(\chi_{c1})$ for prompt χ_c production at $\sqrt{s} = 7$ TeV ☆

LHCb Collaboration

ARTICLE INFO

Article history:
Received 7 February 2012
Received in revised form 18 June 2012
Accepted 28 June 2012
Available online 4 July 2012
Editor: L. Rolandi

ABSTRACT

The prompt production of the charmonium χ_{c1} and χ_{c2} mesons has been studied in proton–proton collisions at the Large Hadron Collider at a centre-of-mass energy of $\sqrt{s} = 7$ TeV. The χ_c mesons are identified through their decays $\chi_c \to J/\psi\gamma$ with $J/\psi \to \mu^+\mu^-$ using 36 pb^{-1} of data collected by the LHCb detector in 2010. The ratio of the prompt production cross-sections for the two χ_c spin states, $\sigma(\chi_{c2})/\sigma(\chi_{c1})$, has been determined as a function of the J/ψ transverse momentum, $p_{\rm T}^{J/\psi}$, in the range from 2 to 15 GeV/c. The results are in agreement with the next-to-leading order non-relativistic QCD model at high $p_{\rm T}^{J/\psi}$ and lie consistently above the pure leading-order colour-singlet prediction.
© 2012 CERN. Published by Elsevier B.V. Open access under CC BY-NC-ND license.

1. Introduction

Explaining heavy quarkonium production remains a challenging problem for Quantum Chromodynamics (QCD). At the energies of the proton–proton (pp) collisions at the Large Hadron Collider, $c\bar{c}$ pairs are expected to be produced predominantly via Leading Order (LO) gluon–gluon interactions, followed by the formation of the bound charmonium states. While the former can be calculated using perturbative QCD, the latter is described by non-perturbative models. Other, more recent, approaches make use of non-relativistic QCD factorisation (NRQCD) which assumes a combination of the colour-singlet (CS) and colour-octet (CO) $c\bar{c}$ and soft gluon exchange for the production of the final bound state [1]. To describe previous experimental data, it was found to be necessary to include Next-to-Leading Order (NLO) QCD corrections for the description of charmonium production [2,3].

The study of the production of P-wave charmonia $\chi_{cJ}(1P)$, with $J = 0, 1, 2$, is important, since these resonances give substantial feed-down contributions to the prompt J/ψ production through their radiative decays $\chi_c \to J/\psi\gamma$ and can have significant impact on the measurement of the J/ψ polarisation. Furthermore, the ratio of the production rate of χ_{c2} to that of χ_{c1} is interesting because it is sensitive to the CS and CO production mechanisms.

Measurements of χ_c production and the relative amounts of the χ_{c1} and χ_{c2} spin states, have previously been made using different particle beams and energies [4–6]. In this Letter, we report a measurement from the LHCb experiment of the ratio of the prompt cross-sections for the two χ_c spin states, $\sigma(\chi_{c2})/\sigma(\chi_{c1})$, as a function of the J/ψ transverse momentum in the range $2 < p_{\rm T}^{J/\psi} < 15$ GeV/c and in the rapidity range $2.0 < y^{J/\psi} < 4.5$. The χ_c candidates are reconstructed through their radiative decay $\chi_c \to J/\psi\gamma$, with $J/\psi \to \mu^+\mu^-$, using a data sample with an integrated luminosity of 36 pb^{-1} collected during 2010. In this Letter, prompt production of χ_c refers to χ_c mesons that are produced at the interaction point and do not arise from the decay of a b-hadron. The sample therefore includes χ_c from the decay of short-lived resonances, such as $\psi(2S)$, which are also produced at the interaction point. All three χ_{cJ} states are considered in the analysis. Since the $\chi_{c0} \to J/\psi\gamma$ branching fraction is ~ 30 (17) times smaller than that of the χ_{c1} (χ_{c2}), the yield of χ_{c0} is not significant. The measurements extend the $p_{\rm T}^{J/\psi}$ coverage with respect to previous experiments.

2. LHCb detector and selection requirements

The LHCb detector [7] is a single-arm forward spectrometer with an angular coverage from approximately 10 mrad to 300 mrad (250 mrad) in the bending (non-bending) plane. The detector consists of a vertex detector (VELO), a dipole magnet, a tracking system, two ring-imaging Cherenkov (RICH) detectors, a calorimeter system and a muon system.

Of particular importance in this measurement are the calorimeter and muon systems. The calorimeter consists of a scintillating pad detector (SPD) and a pre-shower, followed by electromagnetic (ECAL) and hadronic calorimeters. The SPD and pre-shower are designed to distinguish between signals from photons and electrons. The ECAL is constructed from scintillating tiles interleaved with lead tiles. Muons are identified using hits in detectors interleaved with iron filters.

The signal simulation sample used for this analysis was generated using the Pythia 6.4 generator [8] configured with the parameters detailed in Ref. [9]. The EvtGen [10], Photos [11]

☆ © CERN for the benefit of the LHCb Collaboration.

0370-2693/© 2012 CERN. Published by Elsevier B.V. Open access under CC BY-NC-ND license.
http://dx.doi.org/10.1016/j.physletb.2012.06.077

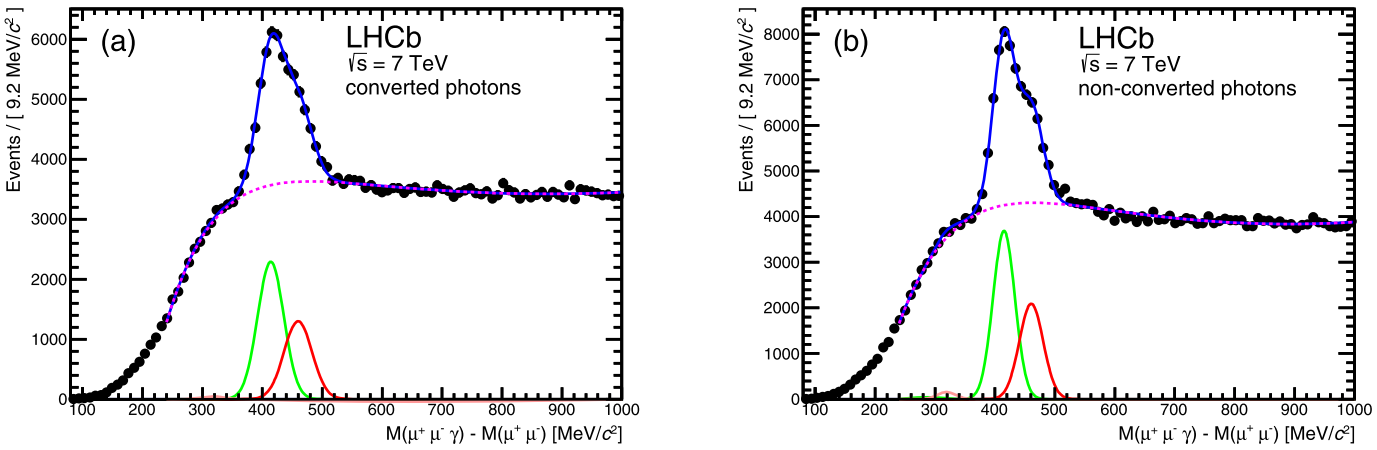


Fig. 1. Distribution of $\Delta M = M(\mu^+\mu^-\gamma) - M(\mu^+\mu^-)$ for selected candidates with $3 < p_{\rm T}^{J/\psi} < 15$ GeV/c for (a) converted and (b) non-converted photons. The lower solid curves correspond to the χ_{c0}, χ_{c1} and χ_{c2} peaks from left to right, respectively (the χ_{c0} peak is barely visible). The background distribution is shown as a dashed curve. The upper solid curve corresponds to the overall fit function.

and GEANT4 [12] packages were used to decay unstable particles, generate QED radiative corrections and simulate interactions in the detector, respectively. The sample consists of events in which at least one $J/\psi \to \mu^+\mu^-$ decay takes place with no constraint on the production mechanism.

The trigger consists of a hardware stage followed by a software stage which applies a full event reconstruction. For this analysis the trigger selects a pair of oppositely charged muon candidates, where either one of the muons has a transverse momentum $p_{\rm T} > 1.8$ GeV/c or one of the pair has $p_{\rm T} > 0.56$ GeV/c and the other has $p_{\rm T} > 0.48$ GeV/c. The invariant mass of the candidates is required to be greater than 2.9 GeV/c^2. The photons are not involved in the trigger decision for this analysis.

Photons are identified and reconstructed using the calorimeter and tracking systems. The identification algorithm provides an estimator for the hypothesis that a calorimeter cluster originates from a photon. This is a likelihood-based estimator constructed from variables that rely on calorimeter and tracking information. For example, in order to reduce the electron background, candidate photon clusters are required not to be matched to a track extrapolated into the calorimeter. For each photon candidate a likelihood (CL_γ) is calculated based on simulated signal and background samples. The photons identified by the calorimeter and used in this analysis can be classified as two types: those that have converted in the material after the dipole magnet and those that have not. Converted photons are identified as clusters in the ECAL with correlated activity in the SPD. In order to account for the different energy resolutions of the two types of photons, the analysis is performed separately for converted and non-converted photons and the results combined as described in Section 3. Photons that convert before the magnet require a different analysis strategy and are not considered here. The photons used to reconstruct the χ_c candidates are required to have a transverse momentum $p_{\rm T}^\gamma > 650$ MeV/c, a momentum $p^\gamma > 5$ GeV/c and a likelihood $\mathrm{CL}_\gamma > 0.5$.

The muon and J/ψ identification criteria are identical to those used in Ref. [13]: each track must be identified as a muon with $p_{\rm T} > 700$ MeV/c and a quality of the track fit $\chi^2/\mathrm{ndf} < 4$, where ndf is the number of degrees of freedom. The two muons must originate from a common vertex with a probability of the vertex fit $> 0.5\%$. In addition, in this analysis the $\mu^+\mu^-$ invariant mass is required to be in the range 3062–3120 MeV/c^2. The J/ψ pseudo-decay time, t_z, is used to reduce the contribution from non-prompt decays, by requiring $t_z = (z_{J/\psi} - z_{\rm PV})M_{J/\psi}/p_z < 0.1$ ps, where $M_{J/\psi}$ is the reconstructed dimuon invariant mass, $z_{J/\psi} - z_{\rm PV}$ is the z separation of the reconstructed production (primary) and decay vertices of the dimuon, and p_z is the z-component of the dimuon momentum with the z-axis parallel to the beam line. Simulation studies show that, with this requirement applied, the remaining fraction of χ_c from b-hadron decays is about 0.1%. This introduces an uncertainty much smaller than any of the other systematic or statistical uncertainties evaluated in this analysis and is not considered further.

In the data, the average χ_c candidate multiplicity per selected event is 1.3 and the percentage of events with more than one genuine χ_c candidate (composed of a unique J/ψ and photon) is estimated to be 0.23% from the simulation. All χ_c candidates are considered for further analysis. The mass difference, $\Delta M = M(\mu^+\mu^-\gamma) - M(\mu^+\mu^-)$, of the selected candidates is shown in Fig. 1 for the converted and non-converted samples; the overlaid fits are described in Section 3.

3. Experimental method

The production cross-section ratio of the χ_{c2} and χ_{c1} states is measured as

$$\frac{\sigma(\chi_{c2})}{\sigma(\chi_{c1})} = \frac{N_{\chi_{c2}}}{N_{\chi_{c1}}} \cdot \frac{\epsilon^{\chi_{c1}}}{\epsilon^{\chi_{c2}}} \cdot \frac{\mathcal{B}(\chi_{c1} \to J/\psi\gamma)}{\mathcal{B}(\chi_{c2} \to J/\psi\gamma)}, \tag{1}$$

where $\mathcal{B}(\chi_{c1} \to J/\psi\gamma)$ and $\mathcal{B}(\chi_{c2} \to J/\psi\gamma)$ are the χ_{c1} and χ_{c2} branching fractions to the final state $J/\psi\gamma$, and

$$\frac{\epsilon^{\chi_{c1}}}{\epsilon^{\chi_{c2}}} = \frac{\epsilon^{\chi_{c1}}_{J/\psi}\epsilon^{\chi_{c1}}_{\gamma}\epsilon^{\chi_{c1}}_{\rm sel}}{\epsilon^{\chi_{c2}}_{J/\psi}\epsilon^{\chi_{c2}}_{\gamma}\epsilon^{\chi_{c2}}_{\rm sel}}, \tag{2}$$

where $\epsilon^{\chi_{cJ}}_{J/\psi}$ is the efficiency to trigger, reconstruct and select a J/ψ from a χ_{cJ} decay, $\epsilon^{\chi_{cJ}}_{\gamma}$ is the efficiency to reconstruct and select a photon from a χ_{cJ} decay and $\epsilon^{\chi_{cJ}}_{\rm sel}$ is the efficiency to subsequently select the χ_{cJ} candidate.

Since the mass difference between the χ_{c1} and χ_{c2} states is 45.54 ± 0.11 MeV/c^2, the signal peaks cannot be separately isolated using the calorimeter information. An unbinned maximum likelihood fit to the ΔM mass difference distribution is performed to obtain the three $N_{\chi_{cJ}}$ yields simultaneously. The determination of the efficiency terms in Eq. (2) is described in Section 3.1.

The signal mass distribution is parametrised using three Gaussian functions ($\mathcal{F}^J_{\rm sig}$ for $J = 0, 1, 2$). The combinatorial background is described by

Table 1
Signal χ_c yields and fit quality from the fit to the converted and non-converted candidates in each $p_T^{J/\psi}$ bin.

$p_T^{J/\psi}$ (GeV/c)	Converted photons			Non-converted photons		
	χ_{c1} yield	χ_{c2} yield	χ^2/ndf	χ_{c1} yield	χ_{c2} yield	χ^2/ndf
2–3	3120 ± 248	2482 ± 301	0.91	4080 ± 246	3927 ± 280	1.02
3–4	3462 ± 224	3082 ± 249	0.81	4919 ± 183	3443 ± 207	1.02
4–5	3235 ± 146	1769 ± 174	1.03	4497 ± 134	2718 ± 143	1.08
5–6	2476 ± 110	1443 ± 121	0.84	3203 ± 105	1999 ± 107	1.45
6–7	1497 ± 80	736 ± 89	1.05	1946 ± 78	1338 ± 83	0.78
7–8	933 ± 77	658 ± 86	0.77	1342 ± 59	747 ± 60	1.15
8–9	660 ± 47	302 ± 51	0.90	817 ± 43	395 ± 42	0.78
9–10	451 ± 34	142 ± 35	0.82	501 ± 32	256 ± 31	1.09
10–11	255 ± 25	86 ± 26	1.13	317 ± 26	188 ± 25	0.85
11–12	129 ± 28	99 ± 30	0.87	222 ± 19	103 ± 18	0.93
12–13	129 ± 16	46 ± 15	1.09	154 ± 15	50 ± 13	0.98
13–15	127 ± 18	42 ± 20	0.91	158 ± 18	63 ± 17	1.05

$$\mathcal{F}_{\rm bgd} = x^a\left(1 - e^{\frac{m_0}{c}(1-x)}\right) + b(x-1), \tag{3}$$

where $x = \Delta M/m_0$ and m_0, a, b and c are free parameters.

A possible source of background from partially reconstructed decays is due to $\psi(2S) \to J/\psi\pi^0\pi^0$ decays where the J/ψ and a photon from one of the neutral pions are reconstructed and selected as a χ_c candidate. Simulation studies show that the expected yield is $\sim 0.1\%$ of the signal yield and this background is therefore neglected for this analysis.

The overall fit function is

$$\mathcal{F} = \sum_{J=0}^{2} f_{\chi_{cJ}} \mathcal{F}_{\rm sig}^{J} + \left[1 - \sum_{J=0}^{2} f_{\chi_{cJ}}\right] \mathcal{F}_{\rm bgd}, \tag{4}$$

where $f_{\chi_{cJ}}$ are the signal fractions. The mass differences between the χ_{c1} and χ_{c2} states and the χ_{c1} and χ_{c0} states are fixed to the values from Ref. [14]. The mass resolutions for the χ_c states, $\sigma_{\rm res}^{\chi_{cJ}}$, are given by the widths of the Gaussian functions for each state. The ratios of the mass resolutions, $\sigma_{\rm res}^{\chi_{c2}}/\sigma_{\rm res}^{\chi_{c1}}$ and $\sigma_{\rm res}^{\chi_{c0}}/\sigma_{\rm res}^{\chi_{c1}}$, are taken from simulation. The value of $\sigma_{\rm res}^{\chi_{c2}}/\sigma_{\rm res}^{\chi_{c1}}$ is consistent with the value measured from data, fitting in a reduced ΔM range and with a simplified background parametrisation.

With the mass differences and the ratio of the mass resolutions fixed, a fit is performed to the data in the range $3 < p_T^{J/\psi} < 15$ GeV/c, in order to determine the χ_{c1} mass resolution $\sigma_{\rm res}^{\chi_{c1}}$. This range is chosen because the background has a different shape in the $p_T^{J/\psi}$ bin 2–3 GeV/c and is not well described by $\mathcal{F}_{\rm bgd}$ when combined with the rest of the sample. Simulation studies show that the signal parameters for the χ_{cJ} states in the $p_T^{J/\psi}$ bin 2–3 GeV/c are consistent with the parameters in the rest of the sample. The distributions of ΔM for the fits to the converted and non-converted candidates are shown in Fig. 1. The mass resolution, $\sigma_{\rm res}^{\chi_{c1}}$, is measured to be 21.8 ± 0.8 MeV/c^2 and 18.3 ± 0.4 MeV/c^2 for converted and non-converted candidates respectively. The corresponding values in the simulation are 19.0 ± 0.2 MeV/c^2 and 17.5 ± 0.1 MeV/c^2 and show a weak dependence of $\sigma_{\rm res}^{\chi_{c1}}$ on $p_T^{J/\psi}$ which is accounted for in the systematic uncertainties.

In order to measure the χ_c yields, the fit is then performed in bins of $p_T^{J/\psi}$ in the range $2 < p_T^{J/\psi} < 15$ GeV/c. For each $p_T^{J/\psi}$ bin, the mass differences, the ratio of the mass resolutions and $\sigma_{\rm res}^{\chi_{c1}}$ are fixed as described above. In total, there are eight free parameters for each fit in each bin in $p_T^{J/\psi}$ and the results are summarised in Table 1; the fit χ^2/ndf for the converted and non-converted samples is good in all bins. The total observed yields of χ_{c0}, χ_{c1} and χ_{c2} are 820 ± 650, $38\,630 \pm 550$ and $26\,110 \pm 620$, respectively, calculated from the signal fractions $f_{\chi_{cJ}}$ and the number of candidates in the sample. The raw χ_c yields for converted and non-converted candidates are combined, corrected for efficiency (as described in Section 3.1) and the cross-section ratio is determined using Eq. (1).

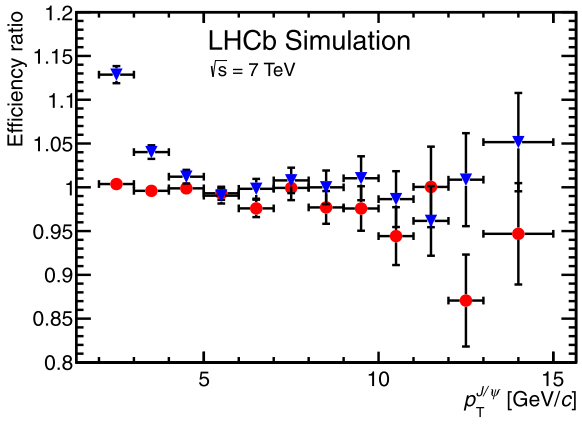


Fig. 2. Reconstruction and selection efficiency ratios in bins of $p_T^{J/\psi}$. The ratio of the J/ψ efficiency ($\epsilon_{J/\psi}^{\chi_{c2}}/\epsilon_{J/\psi}^{\chi_{c1}}$) is shown with red circles. The ratio of the photon reconstruction and selection efficiency times the χ_c selection efficiency ($\epsilon_\gamma^{\chi_{c2}}\epsilon_{\rm sel}^{\chi_{c2}}/\epsilon_\gamma^{\chi_{c1}}\epsilon_{\rm sel}^{\chi_{c1}}$) is shown with blue triangles.

3.1. Efficiencies

The efficiency ratios to reconstruct and select χ_c candidates are obtained from simulation. Since the photon interaction with material is not part of the event generation procedure, the individual efficiencies for converted and non-converted candidates are not separated. Therefore, the combined efficiencies are calculated. The ratios of the overall efficiency for the detection of J/ψ mesons originating from the decay of a χ_{c1} compared to a χ_{c2}, $\epsilon_{J/\psi}^{\chi_{c2}}/\epsilon_{J/\psi}^{\chi_{c1}}$, are consistent with unity for all $p_T^{J/\psi}$ bins, as shown in Fig. 2. The ratios of the efficiencies for reconstructing and selecting photons from χ_c decays and then selecting the χ_c, $\epsilon_\gamma^{\chi_{c2}}\epsilon_{\rm sel}^{\chi_{c2}}/\epsilon_\gamma^{\chi_{c1}}\epsilon_{\rm sel}^{\chi_{c1}}$, are also shown in Fig. 2. In general these efficiency ratios are consistent with unity, except in the $p_T^{J/\psi}$ bins 2–3 GeV/c and 3–4 GeV/c where the reconstruction and detection efficiencies for χ_{c1} are smaller than for χ_{c2}. The increase in the efficiency ratio in these bins arises because the photon p_T spectra are different for χ_{c1} and χ_{c2}. The photon $p_T^\gamma > 650$ MeV/c requirement cuts harder in the case of the χ_{c1} and therefore lowers this efficiency. The increase in the efficiency ratio is a kinematic effect,

Table 2
Polarisation weights in $p_{\mathrm{T}}^{J/\psi}$ bins for different combinations of χ_{c1} and χ_{c2} polarisation states $|J, m_{\chi_{cJ}}\rangle$ with $|m_{\chi_{cJ}}| = 0, \ldots, J$. The polarisation axis is defined as the direction of the χ_c in the laboratory frame. Unpol. means the χ_c is unpolarised.

$(\lvert m_{\chi_{c1}}\rvert, \lvert m_{\chi_{c2}}\rvert)$	$p_{\mathrm{T}}^{J/\psi}$ (GeV/c)											
	2–3	3–4	4–5	5–6	6–7	7–8	8–9	9–10	10–11	11–12	12–13	13–15
(Unpol, 0)	0.99	0.97	0.94	0.91	0.88	0.87	0.86	0.86	0.86	0.85	0.85	0.88
(Unpol, 1)	0.97	0.98	0.97	0.95	0.94	0.94	0.93	0.93	0.93	0.93	0.93	0.93
(Unpol, 2)	1.03	1.04	1.07	1.11	1.14	1.17	1.18	1.18	1.19	1.18	1.19	1.16
(0, Unpol)	1.01	0.99	0.97	0.93	0.90	0.89	0.87	0.86	0.85	0.87	0.86	0.84
(1, Unpol)	0.99	1.00	1.02	1.04	1.05	1.06	1.06	1.07	1.08	1.07	1.07	1.08
(0, 0)	1.00	0.97	0.91	0.84	0.80	0.77	0.75	0.74	0.72	0.74	0.74	0.74
(0, 1)	0.98	0.97	0.93	0.88	0.85	0.83	0.81	0.81	0.79	0.81	0.81	0.78
(0, 2)	1.04	1.03	1.03	1.03	1.03	1.03	1.03	1.02	1.00	1.03	1.03	0.98
(1, 0)	0.99	0.97	0.96	0.94	0.93	0.92	0.92	0.92	0.92	0.91	0.91	0.95
(1, 1)	0.97	0.98	0.98	0.99	0.99	0.99	0.99	1.00	1.00	1.00	1.00	1.01
(1, 2)	1.03	1.04	1.09	1.15	1.20	1.23	1.26	1.26	1.28	1.26	1.27	1.25

rather than a reconstruction effect, and is well modelled by the simulation.

3.2. Polarisation

The production of polarised χ_c states would modify the efficiencies calculated from the simulation, which assumes unpolarised χ_c. A measurement of the χ_c polarisation would require an angular analysis, which is not feasible with the present amount of data. Various polarisation scenarios are considered in Table 2. Assuming no azimuthal dependence in the production process, the $\chi_c \to J/\psi\gamma$ system is described by three angles: $\theta_{J/\psi}$, θ_{χ_c} and ϕ, where $\theta_{J/\psi}$ is the angle between the directions of the positive muon in the J/ψ rest frame and the J/ψ in the χ_c rest frame, θ_{χ_c} is the angle between the directions of the J/ψ in the χ_c rest frame and the χ_c in the laboratory frame, and ϕ is the angle between the plane formed from the χ_c and J/ψ momentum vectors in the laboratory frame and the J/ψ decay plane in the J/ψ rest frame. The angular distributions are independent of the choice of polarisation axis (the direction of the χ_c in the laboratory frame) and are detailed in Ref. [5]. For each simulated event in the unpolarised sample, a weight is calculated from the distribution of these angles in the various polarisation hypotheses compared to the unpolarised distribution. The weights in Table 2 are then the average of these per-event weights in the simulated sample. For a given $(|m_{\chi_{c1}}|, |m_{\chi_{c2}}|)$ polarisation combination, the central value of the determined cross-section ratio in each $p_{\mathrm{T}}^{J/\psi}$ bin should be multiplied by the number in the table. The maximum effect from the possible polarisation of the χ_{c1} and χ_{c2} mesons is given separately from the systematic uncertainties in Table 4 and Fig. 3.

4. Systematic uncertainties

The branching fractions used in the analysis are $\mathcal{B}(\chi_{c1} \to J/\psi\gamma) = 0.344 \pm 0.015$ and $\mathcal{B}(\chi_{c2} \to J/\psi\gamma) = 0.195 \pm 0.008$, taken from Ref. [14]. The relative systematic uncertainty on the cross-section ratio resulting from the $\chi_c \to J/\psi\gamma$ branching fractions is 6%; the absolute uncertainty is given for each bin of $p_{\mathrm{T}}^{J/\psi}$ in Table 3.

The simulation sample used to calculate the efficiencies has approximately the same number of χ_c candidates as are observed in the data. The statistical errors from the finite number of simulated events are included as a systematic uncertainty in the final results. The uncertainty associated to this is determined by sampling the efficiencies used in Eq. (1) according to their errors. The relative systematic uncertainty due to the limited size of the simulation

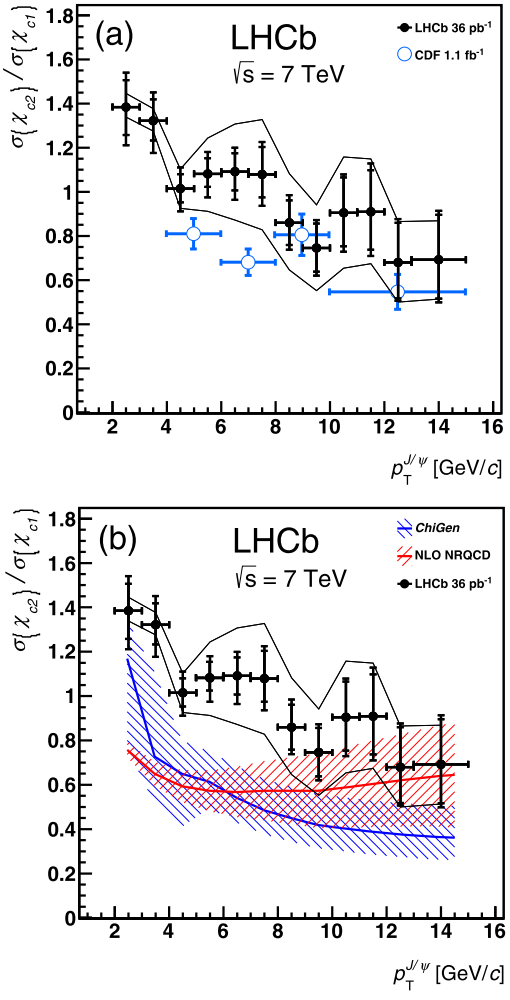


Fig. 3. Ratio $\sigma(\chi_{c2})/\sigma(\chi_{c1})$ in bins of $2 < p_{\mathrm{T}}^{J/\psi} < 15$ GeV/c. The LHCb results, in the rapidity range $2.0 < y^{J/\psi} < 4.5$ and assuming the production of unpolarised χ_c mesons, are shown with solid black circles and the internal error bars correspond to the statistical error; the external error bars include the contribution from the systematic uncertainties (apart from the polarisation). The lines surrounding the data points show the maximum effect of the unknown χ_c polarisations on the result. The upper and lower limits correspond to the spin states as described in the text. The CDF data points, at $\sqrt{s} = 1.96$ TeV in $p\bar{p}$ collisions and in the J/ψ pseudo-rapidity range $|\eta^{J/\psi}| < 1.0$, are shown in (a) with open blue circles [6]. The two hatched bands in (b) correspond to the ChiGen Monte Carlo generator [15] and NLO NRQCD [3] predictions.

Table 3
Summary of the systematic uncertainties (absolute values) on $\sigma(\chi_{c2})/\sigma(\chi_{c1})$ in each $p_T^{J/\psi}$ bin.

$p_T^{J/\psi}$ (GeV/c)	2–3	3–4	4–5	5–6	6–7	7–8
Branching fractions	$^{+0.08}_{-0.08}$	$^{+0.08}_{-0.08}$	$^{+0.06}_{-0.06}$	$^{+0.07}_{-0.07}$	$^{+0.07}_{-0.07}$	$^{+0.06}_{-0.06}$
Size of simulation sample	$^{+0.01}_{-0.01}$	$^{+0.01}_{-0.01}$	$^{+0.01}_{-0.01}$	$^{+0.01}_{-0.01}$	$^{+0.02}_{-0.01}$	$^{+0.02}_{-0.02}$
Fit model	$^{+0.04}_{-0.05}$	$^{+0.05}_{-0.04}$	$^{+0.03}_{-0.03}$	$^{+0.03}_{-0.03}$	$^{+0.03}_{-0.04}$	$^{+0.05}_{-0.04}$
Simulation calibration	$^{+0.00}_{-0.08}$	$^{+0.00}_{-0.07}$	$^{+0.00}_{-0.05}$	$^{+0.00}_{-0.05}$	$^{+0.00}_{-0.06}$	$^{+0.00}_{-0.06}$
$p_T^{J/\psi}$ (GeV/c)	8–9	9–10	10–11	11–12	12–13	13–15
Branching fractions	$^{+0.05}_{-0.05}$	$^{+0.05}_{-0.05}$	$^{+0.05}_{-0.05}$	$^{+0.06}_{-0.06}$	$^{+0.04}_{-0.04}$	$^{+0.04}_{-0.04}$
Size of simulation sample	$^{+0.02}_{-0.02}$	$^{+0.02}_{-0.02}$	$^{+0.04}_{-0.04}$	$^{+0.06}_{-0.06}$	$^{+0.05}_{-0.05}$	$^{+0.05}_{-0.05}$
Fit model	$^{+0.03}_{-0.04}$	$^{+0.03}_{-0.03}$	$^{+0.03}_{-0.03}$	$^{+0.02}_{-0.13}$	$^{+0.02}_{-0.02}$	$^{+0.08}_{-0.03}$
Simulation calibration	$^{+0.00}_{-0.04}$	$^{+0.00}_{-0.04}$	$^{+0.00}_{-0.05}$	$^{+0.00}_{-0.06}$	$^{+0.00}_{-0.04}$	$^{+0.00}_{-0.03}$

Table 4
Ratio $\sigma(\chi_{c2})/\sigma(\chi_{c1})$ in bins of $p_T^{J/\psi}$ in the range $2 < p_T^{J/\psi} < 15$ GeV/c and in the rapidity range $2.0 < y^{J/\psi} < 4.5$. The first error is the statistical error, the second is the systematic uncertainty (apart from the branching fraction and polarisation) and the third is due to the $\chi_c \to J/\psi\gamma$ branching fractions. Also given is the maximum effect of the unknown χ_c polarisations on the result as described in Section 3.2.

$p_T^{J/\psi}$ (GeV/c)	$\sigma(\chi_{c2})/\sigma(\chi_{c1})$	Polarisation effects
2–3	$1.39^{+0.12}_{-0.13}{}^{+0.06}_{-0.09}{}^{+0.08}_{-0.08}$	$^{+0.06}_{-0.05}$
3–4	$1.32^{+0.10}_{-0.09}{}^{+0.03}_{-0.09}{}^{+0.08}_{-0.08}$	$^{+0.06}_{-0.05}$
4–5	$1.02^{+0.07}_{-0.06}{}^{+0.04}_{-0.06}{}^{+0.06}_{-0.06}$	$^{+0.09}_{-0.09}$
5–6	$1.08^{+0.07}_{-0.06}{}^{+0.04}_{-0.06}{}^{+0.07}_{-0.07}$	$^{+0.16}_{-0.17}$
6–7	$1.09^{+0.08}_{-0.09}{}^{+0.03}_{-0.07}{}^{+0.07}_{-0.07}$	$^{+0.22}_{-0.22}$
7–8	$1.08^{+0.13}_{-0.10}{}^{+0.05}_{-0.07}{}^{+0.06}_{-0.06}$	$^{+0.25}_{-0.25}$
8–9	$0.86^{+0.10}_{-0.10}{}^{+0.04}_{-0.06}{}^{+0.05}_{-0.05}$	$^{+0.22}_{-0.21}$
9–10	$0.75^{+0.11}_{-0.11}{}^{+0.04}_{-0.06}{}^{+0.05}_{-0.05}$	$^{+0.20}_{-0.19}$
10–11	$0.91^{+0.16}_{-0.15}{}^{+0.05}_{-0.07}{}^{+0.05}_{-0.05}$	$^{+0.25}_{-0.25}$
11–12	$0.91^{+0.19}_{-0.17}{}^{+0.09}_{-0.10}{}^{+0.06}_{-0.06}$	$^{+0.24}_{-0.24}$
12–13	$0.68^{+0.18}_{-0.16}{}^{+0.05}_{-0.07}{}^{+0.04}_{-0.04}$	$^{+0.19}_{-0.18}$
13–15	$0.69^{+0.20}_{-0.18}{}^{+0.07}_{-0.07}{}^{+0.04}_{-0.04}$	$^{+0.18}_{-0.18}$

sample is found to be in the range (0.6–7.2)% and is given for each $p_T^{J/\psi}$ bin in Table 3.

The measured χ_c yields depend on the values of the fixed parameters and the fit range used. The associated systematic uncertainty has been evaluated by repeating the fit many times, changing the values of the fixed parameters and the fit range. Since the uncertainties arising from the fixed parameters are expected to be correlated, a single procedure is used simultaneously varying all these parameters. The χ_c mass difference parameters are sampled from two Gaussian distributions with widths taken from the errors on the masses given in Ref. [14]. The mass resolution ratios, $\sigma_{\rm res}^{\chi_{c2}}/\sigma_{\rm res}^{\chi_{c1}}$ and $\sigma_{\rm res}^{\chi_{c0}}/\sigma_{\rm res}^{\chi_{c1}}$, are varied according to the error matrix of the fit to the simulated sample in the range $3 < p_T^{J/\psi} < 15$ GeV/c.

The mass resolution $\sigma_{\rm res}^{\chi_{c1}}$ is also determined using a simplified background model and fitting in a reduced range. Simulation studies show that the value of $\sigma_{\rm res}^{\chi_{c1}}$ also has a weak dependence on $p_T^{J/\psi}$. The mass resolution $\sigma_{\rm res}^{\chi_{c1}}$ is randomly sampled from the values obtained from the default fit (described in Section 3) according to its error, the simplified fit, again according to its error, and by modifying it in each $p_T^{J/\psi}$ bin according to the variation observed in the simulation.

The systematic uncertainty associated with the shape of the fitted background function is incorporated by including or excluding the χ_{c0} signal shape, which peaks in the region where the background shape is most sensitive.

The background shape is also sensitive to the rise in the ΔM distribution. The systematic uncertainty from this is included by varying the lower edge of the fit range in the interval ± 10 MeV/c^2 around its nominal value for each bin in $p_T^{J/\psi}$.

The overall systematic uncertainty from the fit is then determined from the distribution of the χ_{c2}/χ_{c1} cross-section ratios by repeating the sampling procedure described above many times. The relative uncertainty is found to be in the range (2.2–14.6)% and is given for each bin of $p_T^{J/\psi}$ in Table 3.

A systematic uncertainty related to the calibration of the simulation is evaluated by performing the analysis on simulated events and comparing the efficiency-corrected ratio of yields, $(N_{\chi_{c2}}/N_{\chi_{c1}}) \cdot (\epsilon^{\chi_{c1}}/\epsilon^{\chi_{c2}})$, to the true ratio generated in the sample. A deviation of -9.6% is observed, caused by non-Gaussian signal shapes in the simulation from the calorimeter calibration. These are not seen in the data, which is well described by Gaussian signal shapes. The deviation is included as a systematic error, by sampling from the negative half of a Gaussian with zero mean and a width of 9.6%. The relative uncertainty on the cross-section ratio is found to be less than 6.0% and is given for each bin of $p_T^{J/\psi}$ in Table 3. A second check of the procedure was performed using simulated events generated according to the distributions observed in the data, *i.e.* three overlapping Gaussians and a background shape similar to that in Fig. 1. In this case no evidence for a deviation was observed. Other systematic uncertainties due to the modelling of the detector in the simulation are negligible.

In summary, the overall systematic uncertainty, excluding that due to the branching fractions, is evaluated by simultaneously sampling the deviation of the cross-section ratio from the central value, using the distributions of the cross-section ratios described above. The separate systematic uncertainties are shown in bins of $p_T^{J/\psi}$ in Table 3 and the combined uncertainties are shown in Table 4.

5. Results and conclusions

The cross-section ratio, $\sigma(\chi_{c2})/\sigma(\chi_{c1})$, measured in bins of $p_T^{J/\psi}$ is given in Table 4 and shown in Fig. 3. Previous measurements from WA11 in π^-Be collisions at 185 GeV/c gave $\sigma(\chi_{c2})/\sigma(\chi_{c1}) = 1.4 \pm 0.6$ [4], and from HERA-B in pA collisions at $\sqrt{s} = 41.6$ GeV with $p_T^{J/\psi}$ below roughly 5 GeV/c gave $\sigma(\chi_{c2})/\sigma(\chi_{c1}) = 1.75 \pm 0.7$ [5]. The data points from CDF [6] at $\sqrt{s} = 1.96$ TeV in $p\bar{p}$ collisions are also shown in Fig. 3(a).

Theoretical predictions, calculated in the LHCb rapidity range $2.0 < y^{J/\psi} < 4.5$, from the ChiGen Monte Carlo generator [15], which is an implementation of the leading-order colour-singlet model described in Ref. [16], and from the NLO NRQCD calculations [3] are shown in Fig. 3(b). The hatched bands represent the uncertainties in the theoretical predictions.

Fig. 3 also shows the maximum effect of the unknown χ_c polarisations on the result, shown as the lines surrounding the data points. In the first $p_{\mathrm{T}}^{J/\psi}$ bin, the upper limit corresponds to the spin state combination $(|m_{\chi c1}|, |m_{\chi c2}|) = (0, 2)$ and the lower limit corresponds to the spin state combination $(1, 1)$. In all subsequent $p_{\mathrm{T}}^{J/\psi}$ bins, the upper limit corresponds to spin state combination $(1, 2)$ and the lower limit corresponds to $(0, 0)$.

In summary, the ratio of the $\sigma(\chi_{c2})/\sigma(\chi_{c1})$ prompt production cross-sections has been measured as a function of $p_{\mathrm{T}}^{J/\psi}$ using 36 pb^{-1} of data collected by LHCb during 2010 at a centre-of-mass energy $\sqrt{s} = 7$ TeV. The ChiGen generator describes the shape of the distribution reasonably well, although the data lie consistently above the model prediction. This could be explained by important higher order perturbative corrections and/or sizeable colour-octet terms not included in the calculation. The results are in agreement with the NLO NRQCD model for $p_{\mathrm{T}}^{J/\psi} > 8$ GeV/c.

Acknowledgements

We would like to thank L.A. Harland-Lang, W.J. Stirling and K. Chao for supplying the theory predictions for comparison to our data and for many helpful discussions.

We express our gratitude to our colleagues in the CERN accelerator departments for the excellent performance of the LHC. We thank the technical and administrative staff at CERN and at the LHCb institutes, and acknowledge support from the National Agencies: CAPES, CNPq, FAPERJ and FINEP (Brazil); CERN; NSFC (China); CNRS/IN2P3 (France); BMBF, DFG, HGF and MPG (Germany); SFI (Ireland); INFN (Italy); FOM and NWO (The Netherlands); SCSR (Poland); ANCS (Romania); MinES of Russia and Rosatom (Russia); MICINN, XuntaGal and GENCAT (Spain); SNSF and SER (Switzerland); NAS Ukraine (Ukraine); STFC (United Kingdom); NSF (USA). We also acknowledge the support received from the ERC under FP7 and the Region Auvergne.

Open access

This article is published Open Access at sciencedirect.com. It is distributed under the terms of the Creative Commons Attribution License 3.0, which permits unrestricted use, distribution, and reproduction in any medium, provided the original authors and source are credited.

References

[1] G.T. Bodwin, E. Braaten, G. Lepage, Phys. Rev. D 51 (1995) 1125, arXiv:hep-ph/9407339;
G.T. Bodwin, E. Braaten, G. Lepage, Phys. Rev. D 55 (1997) 5853 (Erratum).
[2] J.M. Campbell, F. Maltoni, F. Tramontano, Phys. Rev. Lett. 98 (2007) 252002, arXiv:hep-ph/0703113.
[3] Y.-Q. Ma, K. Wang, K.-T. Chao, Phys. Rev. D 83 (2011) 111503, arXiv:1002.3987.
[4] WA11 Collaboration, Y. Lemoigne, et al., Phys. Lett. B 113 (1982) 509;
WA11 Collaboration, Y. Lemoigne, et al., Phys. Lett. B 116 (1982) 470 (Erratum).
[5] HERA-B Collaboration, I. Abt, et al., Phys. Rev. D 79 (2009) 012001, arXiv:0807.2167.
[6] CDF Collaboration, A. Abulencia, et al., Phys. Rev. Lett. 98 (2007) 232001, arXiv:hep-ex/0703028.
[7] LHCb Collaboration, A.A. Alves Jr., et al., JINST 3 (2008) S08005.
[8] T. Sjöstrand, S. Mrenna, P.Z. Skands, JHEP 0605 (2006) 026, arXiv:hep-ph/0603175.
[9] I. Belyaev, et al., IEEE (2010) 1155.
[10] D.J. Lange, Nucl. Instrum. Meth. A 462 (2001) 152.
[11] E. Barberio, Z. Wąs, Comput. Phys. Commun. 79 (1994) 291.
[12] S. Agostinelli, et al., Nucl. Instrum. Meth. A 506 (2003) 250.
[13] LHCb Collaboration, R. Aaij, et al., Eur. Phys. J. C 71 (2011) 1645, arXiv:1103.0423.
[14] Particle Data Group, K. Nakamura, et al., J. Phys. G 37 (2010) 075021, includes 2011 partial update for the 2012 edition.
[15] L.A. Harland-Lang, W.J. Stirling, http://projects.hepforge.org/superchic/chigen.html.
[16] E.W.N. Glover, A.D. Martin, W.J. Stirling, Z. Phys. C 38 (1988) 473;
E.W.N. Glover, A.D. Martin, W.J. Stirling, Z. Phys. C 49 (1991) 526 (Erratum).

LHCb Collaboration

R. Aaij [23], C. Abellan Beteta [35,n], B. Adeva [36], M. Adinolfi [42], C. Adrover [6], A. Affolder [48], Z. Ajaltouni [5], J. Albrecht [37], F. Alessio [37], M. Alexander [47], G. Alkhazov [29], P. Alvarez Cartelle [36], A.A. Alves Jr. [22], S. Amato [2], Y. Amhis [38], J. Anderson [39], R.B. Appleby [50], O. Aquines Gutierrez [10], F. Archilli [18,37], L. Arrabito [53], A. Artamonov [34], M. Artuso [52,37], E. Aslanides [6], G. Auriemma [22,m], S. Bachmann [11], J.J. Back [44], D.S. Bailey [50], V. Balagura [30,37], W. Baldini [16], R.J. Barlow [50], C. Barschel [37], S. Barsuk [7], W. Barter [43], A. Bates [47], C. Bauer [10], Th. Bauer [23], A. Bay [38], I. Bediaga [1], S. Belogurov [30], K. Belous [34], I. Belyaev [30,37], E. Ben-Haim [8], M. Benayoun [8], G. Bencivenni [18], S. Benson [46], J. Benton [42], R. Bernet [39], M.-O. Bettler [17], M. van Beuzekom [23], A. Bien [11], S. Bifani [12], T. Bird [50], A. Bizzeti [17,h], P.M. Bjørnstad [50], T. Blake [37], F. Blanc [38], C. Blanks [49], J. Blouw [11], S. Blusk [52], A. Bobrov [33], V. Bocci [22], A. Bondar [33], N. Bondar [29], W. Bonivento [15], S. Borghi [47,50], A. Borgia [52], T.J.V. Bowcock [48], C. Bozzi [16], T. Brambach [9], J. van den Brand [24], J. Bressieux [38], D. Brett [50], M. Britsch [10], T. Britton [52], N.H. Brook [42], H. Brown [48], A. Büchler-Germann [39], I. Burducea [28], A. Bursche [39], J. Buytaert [37], S. Cadeddu [15], O. Callot [7], M. Calvi [20,j], M. Calvo Gomez [35,n], A. Camboni [35], P. Campana [18,37], A. Carbone [14], G. Carboni [21,k], R. Cardinale [19,37,i], A. Cardini [15], L. Carson [49], K. Carvalho Akiba [2], G. Casse [48], M. Cattaneo [37], Ch. Cauet [9], M. Charles [51], Ph. Charpentier [37], N. Chiapolini [39], K. Ciba [37], X. Cid Vidal [36], G. Ciezarek [49], P.E.L. Clarke [46,37], M. Clemencic [37], H.V. Cliff [43], J. Closier [37], C. Coca [28], V. Coco [23], J. Cogan [6], P. Collins [37], A. Comerma-Montells [35], F. Constantin [28], G. Conti [38], A. Contu [51], A. Cook [42], M. Coombes [42], G. Corti [37], G.A. Cowan [38], R. Currie [46], B. D'Almagne [7], C. D'Ambrosio [37], P. David [8], P.N.Y. David [23], I. De Bonis [4], S. De Capua [21,k], M. De Cian [39], F. De Lorenzi [12], J.M. De Miranda [1], L. De Paula [2], P. De Simone [18],

D. Decamp [4], M. Deckenhoff [9], H. Degaudenzi [38,37], M. Deissenroth [11], L. Del Buono [8], C. Deplano [15], D. Derkach [14,37], O. Deschamps [5], F. Dettori [24], J. Dickens [43], H. Dijkstra [37], P. Diniz Batista [1], F. Domingo Bonal [35,n], S. Donleavy [48], F. Dordei [11], A. Dosil Suárez [36], D. Dossett [44], A. Dovbnya [40], F. Dupertuis [38], R. Dzhelyadin [34], A. Dziurda [25], S. Easo [45], U. Egede [49], V. Egorychev [30], S. Eidelman [33], D. van Eijk [23], F. Eisele [11], S. Eisenhardt [46], R. Ekelhof [9], L. Eklund [47], Ch. Elsasser [39], D. Elsby [55], D. Esperante Pereira [36], L. Estève [43], A. Falabella [16,14,e], E. Fanchini [20,j], C. Färber [11], G. Fardell [46], C. Farinelli [23], S. Farry [12], V. Fave [38], V. Fernandez Albor [36], M. Ferro-Luzzi [37], S. Filippov [32], C. Fitzpatrick [46], M. Fontana [10], F. Fontanelli [19,i], R. Forty [37], M. Frank [37], C. Frei [37], M. Frosini [17,37,f], S. Furcas [20], A. Gallas Torreira [36], D. Galli [14,c], M. Gandelman [2], P. Gandini [51], Y. Gao [3], J.-C. Garnier [37], J. Garofoli [52], J. Garra Tico [43], L. Garrido [35], D. Gascon [35], C. Gaspar [37], N. Gauvin [38], M. Gersabeck [37], T. Gershon [44,37], Ph. Ghez [4], V. Gibson [43,*], V.V. Gligorov [37], C. Göbel [54], D. Golubkov [30], A. Golutvin [49,30,37], A. Gomes [2], H. Gordon [51], M. Grabalosa Gándara [35], R. Graciani Diaz [35], L.A. Granado Cardoso [37], E. Graugés [35], G. Graziani [17], A. Grecu [28], E. Greening [51], S. Gregson [43], B. Gui [52], E. Gushchin [32], Yu. Guz [34], T. Gys [37], G. Haefeli [38], C. Haen [37], S.C. Haines [43], T. Hampson [42], S. Hansmann-Menzemer [11], R. Harji [49], N. Harnew [51], J. Harrison [50], P.F. Harrison [44], J. He [7], V. Heijne [23], K. Hennessy [48], P. Henrard [5], J.A. Hernando Morata [36], E. van Herwijnen [37], E. Hicks [48], K. Holubyev [11], P. Hopchev [4], W. Hulsbergen [23], P. Hunt [51], T. Huse [48], R.S. Huston [12], D. Hutchcroft [48], D. Hynds [47], V. Iakovenko [41], P. Ilten [12], J. Imong [42], R. Jacobsson [37], A. Jaeger [11], M. Jahjah Hussein [5], E. Jans [23], F. Jansen [23], P. Jaton [38], B. Jean-Marie [7], F. Jing [3], M. John [51], D. Johnson [51], C.R. Jones [43], B. Jost [37], M. Kaballo [9], S. Kandybei [40], M. Karacson [37], T.M. Karbach [9], J. Keaveney [12], I.R. Kenyon [55], U. Kerzel [37], T. Ketel [24], A. Keune [38], B. Khanji [6], Y.M. Kim [46], M. Knecht [38], P. Koppenburg [23], A. Kozlinskiy [23], L. Kravchuk [32], K. Kreplin [11], M. Kreps [44], G. Krocker [11], P. Krokovny [11], F. Kruse [9], K. Kruzelecki [37], M. Kucharczyk [20,25,37,j], T. Kvaratskheliya [30,37], V.N. La Thi [38], D. Lacarrere [37], G. Lafferty [50], A. Lai [15], D. Lambert [46], R.W. Lambert [24], E. Lanciotti [37], G. Lanfranchi [18], C. Langenbruch [11], T. Latham [44], C. Lazzeroni [55], R. Le Gac [6], J. van Leerdam [23], J.-P. Lees [4], R. Lefèvre [5], A. Leflat [31,37], J. Lefrançois [7], O. Leroy [6], T. Lesiak [25], L. Li [3], L. Li Gioi [5], M. Lieng [9], M. Liles [48], R. Lindner [37], C. Linn [11], B. Liu [3], G. Liu [37], J.H. Lopes [2], E. Lopez Asamar [35], N. Lopez-March [38], H. Lu [38,3], J. Luisier [38], A. Mac Raighne [47], F. Machefert [7], I.V. Machikhiliyan [4,30], F. Maciuc [10], O. Maev [29,37], J. Magnin [1], S. Malde [51], R.M.D. Mamunur [37], G. Manca [15,d], G. Mancinelli [6], N. Mangiafave [43], U. Marconi [14], R. Märki [38], J. Marks [11], G. Martellotti [22], A. Martens [8], L. Martin [51], A. Martín Sánchez [7], D. Martinez Santos [37], A. Massafferri [1], Z. Mathe [12], C. Matteuzzi [20], M. Matveev [29], E. Maurice [6], B. Maynard [52], A. Mazurov [16,32,37], G. McGregor [50], R. McNulty [12], C. Mclean [14], M. Meissner [11], M. Merk [23], J. Merkel [9], R. Messi [21,k], S. Miglioranzi [37], D.A. Milanes [13,37], M.-N. Minard [4], J. Molina Rodriguez [54], S. Monteil [5], D. Moran [12], P. Morawski [25], R. Mountain [52], I. Mous [23], F. Muheim [46], K. Müller [39], R. Muresan [28,38], B. Muryn [26], B. Muster [38], M. Musy [35], J. Mylroie-Smith [48], P. Naik [42], T. Nakada [38], R. Nandakumar [45], I. Nasteva [1], M. Nedos [9], M. Needham [46], N. Neufeld [37], C. Nguyen-Mau [38,o], M. Nicol [7], V. Niess [5], N. Nikitin [31], A. Nomerotski [51], A. Novoselov [34], A. Oblakowska-Mucha [26], V. Obraztsov [34], S. Oggero [23], S. Ogilvy [47], O. Okhrimenko [41], R. Oldeman [15,d], M. Orlandea [28], J.M. Otalora Goicochea [2], P. Owen [49], K. Pal [52], J. Palacios [39], A. Palano [13,b], M. Palutan [18], J. Panman [37], A. Papanestis [45], M. Pappagallo [47], C. Parkes [47,37], C.J. Parkinson [49], G. Passaleva [17], G.D. Patel [48], M. Patel [49], S.K. Paterson [49], G.N. Patrick [45], C. Patrignani [19,i], C. Pavel-Nicorescu [28], A. Pazos Alvarez [36], A. Pellegrino [23], G. Penso [22,l], M. Pepe Altarelli [37], S. Perazzini [14,c], D.L. Perego [20,j], E. Perez Trigo [36], A. Pérez-Calero Yzquierdo [35], P. Perret [5], M. Perrin-Terrin [6], G. Pessina [20], A. Petrella [16,37], A. Petrolini [19,i], A. Phan [52], E. Picatoste Olloqui [35], B. Pie Valls [35], B. Pietrzyk [4], T. Pilař [44], D. Pinci [22], R. Plackett [47], S. Playfer [46], M. Plo Casasus [36], G. Polok [25], A. Poluektov [44,33], E. Polycarpo [2], D. Popov [10], B. Popovici [28], C. Potterat [35], A. Powell [51], T. du Pree [23], J. Prisciandaro [38], V. Pugatch [41], A. Puig Navarro [35], W. Qian [52], J.H. Rademacker [42], B. Rakotomiaramanana [38], M.S. Rangel [2], I. Raniuk [40], G. Raven [24], S. Redford [51], M.M. Reid [44], A.C. dos Reis [1], S. Ricciardi [45], K. Rinnert [48], D.A. Roa Romero [5], P. Robbe [7], E. Rodrigues [47,50], F. Rodrigues [2], P. Rodriguez Perez [36], G.J. Rogers [43], S. Roiser [37], V. Romanovsky [34], M. Rosello [35,n], J. Rouvinet [38], T. Ruf [37], H. Ruiz [35], G. Sabatino [21,k], J.J. Saborido Silva [36], N. Sagidova [29], P. Sail [47], B. Saitta [15,d], C. Salzmann [39], M. Sannino [19,i], R. Santacesaria [22], C. Santamarina Rios [36], R. Santinelli [37], E. Santovetti [21,k], M. Sapunov [6], A. Sarti [18,l], C. Satriano [22,m], A. Satta [21], M. Savrie [16,e],

D. Savrina [30], P. Schaack [49], M. Schiller [24], S. Schleich [9], M. Schlupp [9], M. Schmelling [10], B. Schmidt [37], O. Schneider [38], A. Schopper [37], M.-H. Schune [7], R. Schwemmer [37], B. Sciascia [18], A. Sciubba [18,l], M. Seco [36], A. Semennikov [30], K. Senderowska [26], I. Sepp [49], N. Serra [39], J. Serrano [6], P. Seyfert [11], B. Shao [3], M. Shapkin [34], I. Shapoval [40,37], P. Shatalov [30], Y. Shcheglov [29], T. Shears [48], L. Shekhtman [33], O. Shevchenko [40], V. Shevchenko [30], A. Shires [49], R. Silva Coutinho [44], T. Skwarnicki [52], A.C. Smith [37], N.A. Smith [48], E. Smith [51,45], K. Sobczak [5], F.J.P. Soler [47], A. Solomin [42], F. Soomro [18], B. Souza De Paula [2], B. Spaan [9], A. Sparkes [46], P. Spradlin [47], F. Stagni [37], S. Stahl [11], O. Steinkamp [39], S. Stoica [28], S. Stone [52,37], B. Storaci [23], M. Straticiuc [28], U. Straumann [39], V.K. Subbiah [37], S. Swientek [9], M. Szczekowski [27], P. Szczypka [38], T. Szumlak [26], S. T'Jampens [4], E. Teodorescu [28], F. Teubert [37], C. Thomas [51], E. Thomas [37], J. van Tilburg [11], V. Tisserand [4], M. Tobin [39], S. Topp-Joergensen [51], N. Torr [51], E. Tournefier [4,49], M.T. Tran [38], A. Tsaregorodtsev [6], N. Tuning [23], M. Ubeda Garcia [37], A. Ukleja [27], P. Urquijo [52], U. Uwer [11], V. Vagnoni [14], G. Valenti [14], R. Vazquez Gomez [35], P. Vazquez Regueiro [36], S. Vecchi [16], J.J. Velthuis [42], M. Veltri [17,g], B. Viaud [7], I. Videau [7], X. Vilasis-Cardona [35,n], J. Visniakov [36], A. Vollhardt [39], D. Volyanskyy [10], D. Voong [42], A. Vorobyev [29], H. Voss [10], S. Wandernoth [11], J. Wang [52], D.R. Ward [43], N.K. Watson [55], A.D. Webber [50], D. Websdale [49], M. Whitehead [44], D. Wiedner [11], L. Wiggers [23], G. Wilkinson [51], M.P. Williams [44,45], M. Williams [49], F.F. Wilson [45], J. Wishahi [9], M. Witek [25], W. Witzeling [37], S.A. Wotton [43], K. Wyllie [37], Y. Xie [46], F. Xing [51], Z. Xing [52], Z. Yang [3], R. Young [46], O. Yushchenko [34], M. Zavertyaev [10,a], F. Zhang [3], L. Zhang [52], W.C. Zhang [12], Y. Zhang [3], A. Zhelezov [11], L. Zhong [3], E. Zverev [31], A. Zvyagin [37]

[1] *Centro Brasileiro de Pesquisas Físicas (CBPF), Rio de Janeiro, Brazil*
[2] *Universidade Federal do Rio de Janeiro (UFRJ), Rio de Janeiro, Brazil*
[3] *Center for High Energy Physics, Tsinghua University, Beijing, China*
[4] *LAPP, Université de Savoie, CNRS/IN2P3, Annecy-Le-Vieux, France*
[5] *Clermont Université, Université Blaise Pascal, CNRS/IN2P3, LPC, Clermont-Ferrand, France*
[6] *CPPM, Aix-Marseille Université, CNRS/IN2P3, Marseille, France*
[7] *LAL, Université Paris-Sud, CNRS/IN2P3, Orsay, France*
[8] *LPNHE, Université Pierre et Marie Curie, Université Paris Diderot, CNRS/IN2P3, Paris, France*
[9] *Fakultät Physik, Technische Universität Dortmund, Dortmund, Germany*
[10] *Max-Planck-Institut für Kernphysik (MPIK), Heidelberg, Germany*
[11] *Physikalisches Institut, Ruprecht-Karls-Universität Heidelberg, Heidelberg, Germany*
[12] *School of Physics, University College Dublin, Dublin, Ireland*
[13] *Sezione INFN di Bari, Bari, Italy*
[14] *Sezione INFN di Bologna, Bologna, Italy*
[15] *Sezione INFN di Cagliari, Cagliari, Italy*
[16] *Sezione INFN di Ferrara, Ferrara, Italy*
[17] *Sezione INFN di Firenze, Firenze, Italy*
[18] *Laboratori Nazionali dell'INFN di Frascati, Frascati, Italy*
[19] *Sezione INFN di Genova, Genova, Italy*
[20] *Sezione INFN di Milano Bicocca, Milano, Italy*
[21] *Sezione INFN di Roma Tor Vergata, Roma, Italy*
[22] *Sezione INFN di Roma La Sapienza, Roma, Italy*
[23] *Nikhef National Institute for Subatomic Physics, Amsterdam, The Netherlands*
[24] *Nikhef National Institute for Subatomic Physics and Vrije Universiteit, Amsterdam, The Netherlands*
[25] *Henryk Niewodniczanski Institute of Nuclear Physics, Polish Academy of Sciences, Kraców, Poland*
[26] *AGH University of Science and Technology, Kraców, Poland*
[27] *Soltan Institute for Nuclear Studies, Warsaw, Poland*
[28] *Horia Hulubei National Institute of Physics and Nuclear Engineering, Bucharest-Magurele, Romania*
[29] *Petersburg Nuclear Physics Institute (PNPI), Gatchina, Russia*
[30] *Institute of Theoretical and Experimental Physics (ITEP), Moscow, Russia*
[31] *Institute of Nuclear Physics, Moscow State University (SINP MSU), Moscow, Russia*
[32] *Institute for Nuclear Research of the Russian Academy of Sciences (INR RAN), Moscow, Russia*
[33] *Budker Institute of Nuclear Physics (SB RAS) and Novosibirsk State University, Novosibirsk, Russia*
[34] *Institute for High Energy Physics (IHEP), Protvino, Russia*
[35] *Universitat de Barcelona, Barcelona, Spain*
[36] *Universidad de Santiago de Compostela, Santiago de Compostela, Spain*
[37] *European Organization for Nuclear Research (CERN), Geneva, Switzerland*
[38] *Ecole Polytechnique Fédérale de Lausanne (EPFL), Lausanne, Switzerland*
[39] *Physik-Institut, Universität Zürich, Zürich, Switzerland*
[40] *NSC Kharkiv Institute of Physics and Technology (NSC KIPT), Kharkiv, Ukraine*
[41] *Institute for Nuclear Research of the National Academy of Sciences (KINR), Kyiv, Ukraine*
[42] *H.H. Wills Physics Laboratory, University of Bristol, Bristol, United Kingdom*
[43] *Cavendish Laboratory, University of Cambridge, Cambridge, United Kingdom*
[44] *Department of Physics, University of Warwick, Coventry, United Kingdom*
[45] *STFC Rutherford Appleton Laboratory, Didcot, United Kingdom*
[46] *School of Physics and Astronomy, University of Edinburgh, Edinburgh, United Kingdom*
[47] *School of Physics and Astronomy, University of Glasgow, Glasgow, United Kingdom*
[48] *Oliver Lodge Laboratory, University of Liverpool, Liverpool, United Kingdom*
[49] *Imperial College London, London, United Kingdom*
[50] *School of Physics and Astronomy, University of Manchester, Manchester, United Kingdom*

[51] *Department of Physics, University of Oxford, Oxford, United Kingdom*
[52] *Syracuse University, Syracuse, NY, United States*
[53] *CC-IN2P3, CNRS/IN2P3, Lyon-Villeurbanne, France* [p]
[54] *Pontifícia Universidade Católica do Rio de Janeiro (PUC-Rio), Rio de Janeiro, Brazil* [q]
[55] *University of Birmingham, Birmingham, United Kingdom*

* Corresponding author.
E-mail address: gibson@hep.phy.cam.ac.uk (V. Gibson).
[a] P.N. Lebedev Physical Institute, Russian Academy of Science (LPI RAS), Moscow, Russia.
[b] Università di Bari, Bari, Italy.
[c] Università di Bologna, Bologna, Italy.
[d] Università di Cagliari, Cagliari, Italy.
[e] Università di Ferrara, Ferrara, Italy.
[f] Università di Firenze, Firenze, Italy.
[g] Università di Urbino, Urbino, Italy.
[h] Università di Modena e Reggio Emilia, Modena, Italy.
[i] Università di Genova, Genova, Italy.
[j] Università di Milano Bicocca, Milano, Italy.
[k] Università di Roma Tor Vergata, Roma, Italy.
[l] Università di Roma La Sapienza, Roma, Italy.
[m] Università della Basilicata, Potenza, Italy.
[n] LIFAELS, La Salle, Universitat Ramon Llull, Barcelona, Spain.
[o] Hanoi University of Science, Hanoi, Viet Nam.
[p] Associated member: CC-IN2P3, CNRS/IN2P3, Lyon-Villeurbanne, France.
[q] Associated to: Pontifícia Universidade Católica do Rio de Janeiro (PUC-Rio), Rio de Janeiro, Brazil.